Research Article Vol. 30, No. 23 / 7 Nov 2022 / Optics Express 41847
Optics EXPRESS

Suppressing the polarization aberrations by combining reflection and refraction optical groups

CHUNMING JIANG,[1,2] DONG YAO,[1,3,*] LINGTONG MENG,[1,3] CHUNHUI YAN,[1,3] AND HONGHAI SHEN[1,3]

[1] Chinese Academy of Science, Changchun Institute of Optics, Fine Mechanics and Physics, Changchun, Jilin 130033, China
[2] University of Chinese Academy of Sciences, Beijing 100049, China
[3] Key laboratory of Airborne Optical Imaging and Measurement, Chinese Academy of Sciences, Changchun 130033, China
[*] 171502099@qq.com

Abstract: Polarization remote sensing technology expands the dimensions of the target and enriches its basic information over traditional remote sensing methods. During the imaging process, polarization imaging changes the polarization information of the target by the modulation of the optical system, affecting the detection accuracy. We term the modulation of the polarization state of light by an optical system as polarization aberration, and we found that a lens group combined with mirrors is beneficial in suppressing polarization aberrations. This study analyzed the principles of suppression and the polarization aberration of the optical system before and after suppression. Simulation results show that the diattenuation's average value is reduced by 51.1% and the retardance's average value is reduced by 26.3% after suppression. The corrected polarization cross-coupled energy is reduced by 73.18% in the central field of view and by 69.80% in the fringe field of view. Adding a lens group also effectively suppresses traditional aberrations and expands the field of view.

1. Introduction

When polarized light propagates in optical systems; the transmission coefficients of the optical medium surface to S and P light are different, and this difference changes to a certain extent every time the incident light passes through the optical medium owing to the difference in the angle of incidence and the material of the medium. The polarization change caused by the optical system can be represented by a Jones matrix, and deviations from this identity matrix are referred to as polarization aberrations [1].

In some high-resolution optical instruments, polarization aberrations limit the image quality: when using astronomical telescopes to observe faint exoplanets, the polarization aberrations of the optical system can generate "ghost" PSF images, the radius of the spatial extent of the 90% encircled energy of these two ghost PSF image is twice as large as the radius of the Airy diffraction pattern, which will interfere with exoplanets measurements [2–4]. The evolution of lithography is one of the key drivers for advancing semiconductor technology nodes. To approximately transfer the mask pattern to the photoresist, the image quality of the lithographic lens must meet extremely demanding requirements. The advancement of integrated circuit nodes promotes a continuous increase in the numerical aperture (NA) of the lithography objective lens. When NA increases to a certain level, the polarization state of the imaging beam has a non-negligible effect on the imaging quality, and polarization aberrations must be considered [5–7]. Similarly, polarization aberrations cause undesirable polarization components (depolarization) that reduce extinction in the image plane in a high-NA microscope imaging system. The polarization aberrations result

#472316 https://doi.org/10.1364/OE.472316
Journal © 2022 Received 3 Aug 2022; revised 24 Sep 2022; accepted 25 Sep 2022; published 28 Oct 2022

Optics EXPRESS

in four bright quadrants separated by a dark cross, known as the Maltese cross, which is seen in the exit pupil of a high-numerical-aperture (NA) [8]. This study aimed to design a weak polarization aberration lens for accurate remote sensing of polarization information. The lens has the characteristics of high spatial resolution, small size, and large field of view.

Some optical design methods for suppressing polarization aberrations have been proposed. Banerjee modeled an optical system with six aluminum-coated folding mirrors to suppress linear diattenuation and retardance [9]. Chipman proposed that the polarization aberrations of a fold mirror can be compensated by orienting the second fold mirror's P-polarization with the S-polarization of the first mirror [10]. However, this method only confirms the theoretical feasibility and does not provide an actual optical system nor does it analyze the balance between polarization aberrations and conventional aberrations. Jia designed a reflective coating to reduce the effects of polarization aberrations [11]. We needed a telescope with a small size and a large field of view, which is difficult to achieve in a reflecting telescope; therefore, we designed a catadioptric telescope. The results show that the addition of the lens group can not only correct traditional aberrations but also suppress polarization aberrations.

In this study, we analyzed the amplitude response curves of different materials to S and P light at different incident angles and found that the reflectance of the metal coating medium to S light is always higher than that of P light, whereas the transmittance of the glass medium to S light is always less than that of P light. Based on this discovery, a design method that combines reflection and refraction optical groups to reduce polarization aberrations is proposed. optimizer balances the polarization aberrations, wavefront aberrations, and other constraints to complete the optical design. A method for calculating the polarization cross-coupled energy caused by polarization aberrations is proposed by using the orientation Zernike polynomials, and the polarization cross-coupled energy before and after adding the lens group was analyzed. The results showed that the cross-coupled energy was reduced 69.80%–73.18% in the full field of view after suppression, and the MTF of the system was also significantly improved after adding the lens.

2. Principles and methods

2.1. Polarization aberrations description

Lenses and reflective mirrors are weakly polarized elements. According to Fresnel's law, the reflective and refractive coefficients of S-polarized light and P-polarized light are characterized by [12]

$$\begin{cases} r_s = -\frac{sin(\theta_1-\theta_2)}{sin(\theta_1+\theta_2)} = |r_s|\, e^{i\varphi_{rs}} \\ r_p = \frac{tan(\theta_1-\theta_2)}{tan(\theta_1+\theta_2)} = \left|r_p\right| e^{i\varphi_{rp}} \\ t_s = \frac{2sin\theta_2 cos\theta_1}{sin(\theta_1+\theta_2)} = |t_s|\, e^{i\varphi_{ts}} \\ t_p = \frac{2sin\theta_2 cos\theta_1}{sin(\theta_1+\theta_2)cos(\theta_1-\theta_2)} = \left|t_p\right| e^{i\varphi_{tp}} \end{cases}, \tag{1}$$

where r_s is the reflective coefficient of S-polarized light; r_p is the reflective coefficient of P-polarized light; t_s is the refractive coefficient of S-polarized light; t_p is the refractive coefficient of P-polarized light; θ_1 is the angle of incidence; and θ_2 is the angle of refraction.

The difference in the reflective and transmissive coefficients between S light and P light changes the polarization state of incident light. Diattenuation is used to measure the difference in S and P light transmittance [13]

$$D = \frac{\left|\alpha_s^2 - \alpha_p^2\right|}{\left|\alpha_s^2 + \alpha_p^2\right|}, \tag{2}$$

where α represents reflective coefficient in reflective mirror surface and refractive coefficient in lenses surface. The retardance characterizes the phase difference between two orthogonal

Optics EXPRESS

polarization components

$$\delta = \left|\varphi_s - \varphi_p\right|. \tag{3}$$

If the polarized light is received by a telescope, the amplitude and phase of the two orthogonal polarization components may be different, and the change in the polarization state of the incident light by the optical system is called polarization aberrations.

A 2×2 Jones matrix at the exit pupil position can be used to describe the polarization aberrations function of the optical system. The matrix can be obtained by tracing polarized rays. The Jones pupil can be expressed as

$$J(H,\rho,\lambda) = \begin{bmatrix} J_{xx}(H,\rho,\lambda) & J_{xy}(H,\rho,\lambda) \\ J_{yx}(H,\rho,\lambda) & J_{yy}(H,\rho,\lambda) \end{bmatrix}, \tag{4}$$

where H is the object coordinate, ρ is the pupil coordinate, and λ is the wavelength. Jones matrices contain complex components with amplitudes and phases.

In conventional scalar imaging theory, the point spread function (PSF) is calculated by taking the Fourier transform of the wavefront function of the exit pupil and assuming that the amplitude and phase response of S and P light are consistent. However, in sensitive polarization systems, changes in the polarization state of light must be taken into account. The amplitude response matrix(ARM), obtained by the spatial Fourier transform of the Jones pupil, is proposed to describe the amplitude distribution on the imaging plane after the polarized beam passes through the optical system [14],

$$ARM = \begin{bmatrix} \mathcal{F}[J_{xx}(H,\rho,\lambda)] & \mathcal{F}[J_{xy}(H,\rho,\lambda)] \\ \mathcal{F}[J_{yx}(H,\rho,\lambda)] & \mathcal{F}[J_{yy}(H,\rho,\lambda)] \end{bmatrix}, \tag{5}$$

where F is the sign of the Fourier transform, and for a beam of polarized light with a fixed polarization direction, the energy distribution at the focal plane is the superposition of the product of the ARM and incident light Jones matrix. The ARM for the catadioptric cassegrain telescope system is shown in Fig. 1.

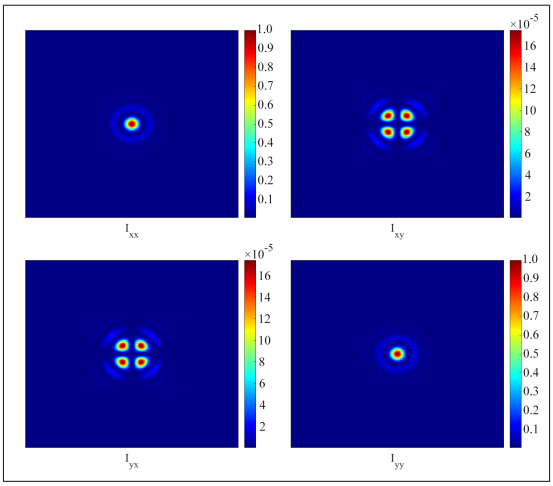

Fig. 1. The light intensity of the 2×2 ARM at an on-axis field point is shown for the example telescope of Fig. 5 normalized by the peak of the XX-component

For unpolarized illumination, the incident X- and Y-polarizations are incoherent with respect to each other. Hence, the output components ARM_{XX} (X in X out) and ARM_{YX} (X in Y out) are

Optics EXPRESS

coherent with each other but incoherent with ARM_{XY} and ARM_{YY}. Therefore, the point spread function for an unpolarized source with four additive components,

$$I = I_{XX} + I_{YX} + I_{XY} + I_{YY} = |ARM_{XX}|^2 + |ARM_{YX}|^2 + |ARM_{XY}|^2 + |ARM_{YY}|^2 . \tag{6}$$

In Fig. 1, the diagonal elements are close to the well-known Airy disk pattern, but the off-diagonal elements have much lower intensity and are shown in a Maltese cross pattern. We refer to these off-diagonal PSF images as the ghost PSFs. The ghost PSFs reduces the imaging resolution, and it is necessary to take effective measures to reduce the influence of polarization aberrations.

2.2. Polarization aberrations suppression

According to the Fresnel formula

$$\frac{|t_s|}{|t_p|} = |cos(\theta_1 - \theta_2)| , \tag{7}$$

where θ_1 is the angle of incidence and θ_2 is the angle of refraction. If θ_1 and θ_2 are equal, then the transmittance of S light is equal to that of P light, and the diattenuation is 0. However, in an optical system, this is impossible. Therefore, when light is refracted in the lens, the transmittance of S light is always lower than that of P light. Light reflected and refracted from the surface of the medium satisfies the law of energy conservation, that is,

$$\begin{cases} R_S + T_S = 1 \\ R_P + T_P = 1 \end{cases} . \tag{8}$$

Therefore, when light is reflected from the surface of the medium, the reflectivity of S light is always greater than that of P light. We analyzed the relationship between the transmittance, phase and the angle of incidence, as shown in Fig. 2.

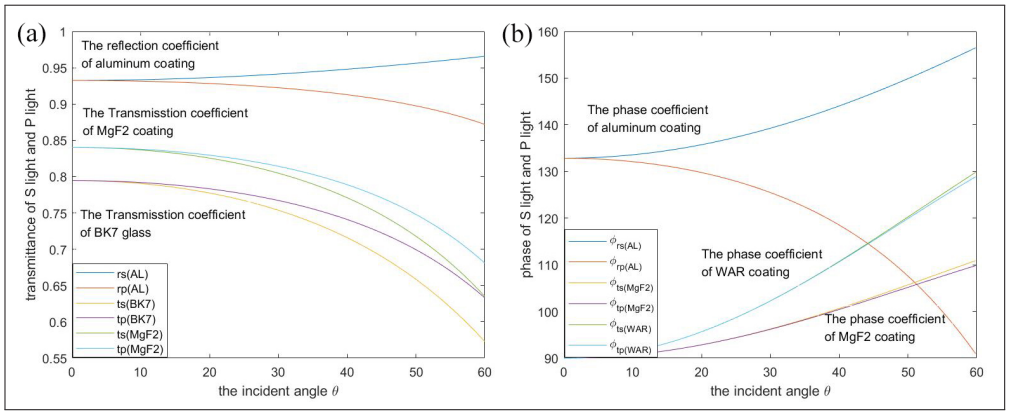

Fig. 2. (a)Reflectance of S light and P light on the metal surface and the transmittance on the lens and AR coated surface. (b)Phase of S light and P light on the metal surface and AR coating surface

Figure 2 shows the change in the polarization state of light in three typical materials as light propagates through an optical system. The reflectance of S light on the metal surface is always greater than that of P light, while the transmittance of S light on the lens surface and

Optics EXPRESS

anti-reflection coating is always less than that of P light. The metal surface has a great influence on the retardance, while the anti-reflection coating basically does not change the retardance. We can adjust the incident angle of the light on the mirror appropriately to reduce the retardance. When a beam of light passes through the reflection optical group, its reflection coefficient satisfies

$$\frac{|r_s|}{|r_p|} = k, \tag{9}$$

k is the scale factor. In the Cartesian coordinate system, when a refractive optical group is added and the light has no polarization aberration, the Jones matrix satisfies

$$\begin{aligned} J_{dia}(d,\theta) &= \begin{bmatrix} cos\theta & -sin\theta \\ sin\theta & cos\theta \end{bmatrix} \begin{bmatrix} 1+d & 0 \\ 0 & 1-d \end{bmatrix} \begin{bmatrix} cos\theta & sin\theta \\ -sin\theta & cos\theta \end{bmatrix} \\ &= \begin{bmatrix} 1+dcos2\theta & dsin2\theta \\ dsin2\theta & 1-dcos2\theta \end{bmatrix} = \begin{bmatrix} 1 & 0 \\ 0 & 1 \end{bmatrix}, \end{aligned} \tag{10}$$

d represents the relative amplitude difference and θ represents the angle between the incident plane and the meridian plane, respectively. Then, the polarized light refracting in the lens should satisfy

$$\frac{|t_s|}{|t_p|} = |\cos(\theta_1 - \theta_2)| = \frac{1}{k}. \tag{11}$$

The optical path of the light entering the lens is shown in Fig. 3.

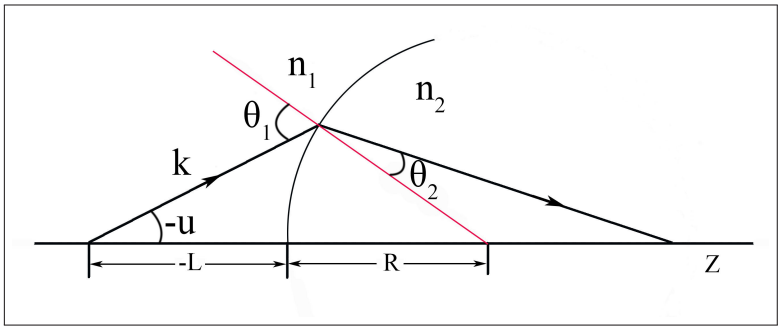

Fig. 3. Optical path diagram of light refracted on the lens surface

The positive and negative symbols in the figure satisfy the law of symbols; it can be seen that

$$\cos(-u) = \frac{\vec{k} \cdot \vec{Z}}{|k|\,|Z|}, \tag{12}$$

from the trigonometric relationship,

$$\frac{\sin(-u)}{r} = \frac{\sin(180^\circ - \theta_1)}{r-L} = \frac{\sin(\theta_1)}{r-L}, \tag{13}$$

$$\sin(\theta_1) = \frac{L-r}{r}\sin(u), \tag{14}$$

by Snell's law

$$n_1 \sin(\theta_1) = n_2 \sin(\theta_2), \tag{15}$$

Optics EXPRESS

$$\sin(\theta_2) = \frac{n_1}{n_2}\frac{L-r}{r}\sin(u). \tag{16}$$

For convenience of calculation, we let

$$\begin{cases} N = \frac{n_1}{n_2} \\ M = \frac{L-r}{r} \end{cases}. \tag{17}$$

Expanding Eqs. (14) and (16) using the Taylor formula, we obtain

$$\theta_1 = Mu + \frac{1}{6}M(M^2-1)u^3, \tag{18}$$

$$\theta_2 = NMu + \frac{1}{6}NM(N^2M^2-1)u^3. \tag{19}$$

Substituting Eqs. (18) and (19) into Eq. (11), the formula for correcting the polarization aberration becomes

$$Mu(1-N)[1 + \frac{1}{6}u^2M^2(1+N^2+N) - \frac{1}{6}u^2] = \arccos(\frac{1}{k}). \tag{20}$$

When the relative refractive index N, radius of curvature r of the medium, and distance L between the medium and reflected mirror satisfy the relationship in Eq. (20), the diattenuation can be suppressed well. In an actual optical system, the coefficient k is assigned to the surfaces of multiple lenses and an anti-reflection coating. The optical design software changes the radius of curvature and the thickness of the lens to satisfy Eq. (20). We also wanted to correct the retardance through the lens group; however, the retardance was caused by the index of the metal reflective coating being a complex number, and the index of the lens is a real number that cannot correct the retardance. However, reducing the incident angle of the light on the metal surface can reduce the retardance to a certain extent.

To design an optical system, a merit function is typically designed to characterize the wavefront and image quality, and an optimization program adjusts the constructional parameters of the system to find acceptable configurations. We designed an optimization evaluation function,

$$\Phi^2 = \frac{w_1\phi_{effl}^2 + w_2\phi_{lens}^2 + w_3\phi_{trac}^2 + w_4\phi_{spha}^2 + w_5\phi_{coma}^2 + w_6\phi_{diat}^2}{w_1 + w_2 + w_3 + w_4 + w_5 + w_6}, \tag{21}$$

w represents the weight, ϕ_{effl} represents the limit of focal length, ϕ_{lens} represents the constraints on the lens boundary conditions, ϕ_{trac} the vertical axis aberration on the image plane, ϕ_{spha}

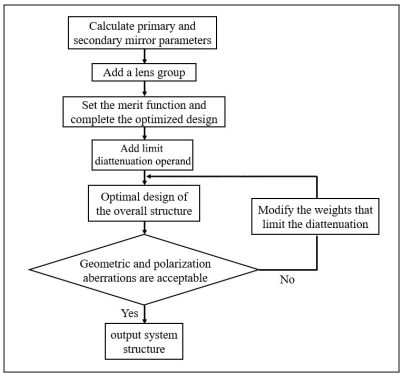

Fig. 4. Optical system design flow chart

Optics EXPRESS

represents spherical aberration, ϕ_{coma} represents coma aberration and ϕ_{diat} represents the limit on polarization aberration related to Eq. (20) that we write in macro language. The design process is illustrated in Fig. 4.

3. Results and analysis

3.1. Optical system design results

In this study, two different design results were obtained by continuously changing the weight factor w_6 which limits the diattenuation to 1 and 2. The system consisted of two reflective mirrors and four lenses with a focal length of 431mm and an F number of 4.31. The wavelength we analyzed was 500 nm, the coating of all mirrors was bare metal aluminum with a complex refractive index of n = 0.916 + 1.84i, and the field of view of this optical system was 1°×1°. Table 1 describes the main optical parameters of the Cassegrain telescope system. Design results as we show in Code 1 (Ref. [15]).

Table 1. Optical parameters of Cassegrain telescopes with different design structures

surf	Radius(mm)			Thickness(mm)			Material	Conic k	Coating
	design 1	design 2	design 3	design 1	design 2	design 3			
M1	−248.4	−291.3	−294.9	−87.0	−87.0	−87.0	Mirror	−1.119754	Aluminum
M2	−116.9	−196.7	−197.3	102.1	50.0	50.0	Mirror	−5	Aluminum
L1R1		87.2	394.3		5.0	3.4	H-K9L		MGF2
L1R2		380.7	−70.4		6.8	5.1			MGF2
L2R1		223.9	−72.9		5.0	3.6	H-K51		MGF2
L2R2		44.6	−341.7		10.0	2.4			MGF2
L3R1		115.9	−92.5		4.9	4.8	ZF1		MGF2
L3R2		303.6	−72.5		0.5	6.5			MGF2
L4R1		50.0	53.4		2.0	4.2	H-K51		MGF2
L4R2		39.1	32.9		73.1	77.1			MGF2

The structures of the three design results are shown in Fig. 5.

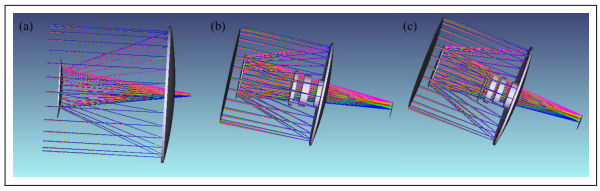

Fig. 5. Cassegrain telescope system structure

3.2. Suppression of diattenuation

We analyzed the polarization aberrations of the system before and after the suppression. To demonstrate a physically intuitive interpretation of the Jones matrix, the singular value decomposition (SVD) theorem is used to decompose the Jones matrix into two parts,

$$J = UDV^{\dagger} = (UDU^{\dagger})(UV^{\dagger}), \tag{22}$$

where † is the sign of the conjugate transpose, $UDU^{\dagger}$ is a Hermitian matrix associated with diattenuation aberration, $UV^{\dagger}$ is a unitary matrix associated with retardance aberration.

Optics EXPRESS

The diattenuation and retardance distribution of the central field of view for the three design results is shown in Fig. 6, where the length of the line and the color of the line position represent the value of diattenuation and retardance, the orientation of the line shows the axis of maximum transmission in diattenuation pupil and the fast axis in retardance pupil. Both before and after suppression, the diattenuation and retardance gradually increases from the center to the edge because as the incident angle increases, the difference between the transmission and phase coefficients of S and P light gradually increases, as shown in Fig. 2. As shown in Fig. 6, with an increase in the weight factor for suppressing diattenuation, the diattenuation of the optical system is gradually suppressed. The maximum diattenuation of the system caused by the two reflective mirrors is 4.44% and the average value of diattenuation is 2.27% in design 1, after use lenses group suppression in design 3, the maximum diattenuation of the entire system is 2.09% and the average value of diattenuation is 1.11%. The maximum retardance of the system caused by the two reflective mirrors is 1.58% and the average value of retardance is 0.8% in design 1, the maximum retardance of the entire system is 1.16% and the average value is 0.59%. When unpolarized light, such as starlight, is incident, diattenuation is equal to the degree of polarization (DoP) of the exiting light. Because of the diattenuation and retardance, light incident in states different from S and P have some fraction of the energy coupled into the orthogonal polarization, and reducing the diattenuation can effectively reduce the coupled energy [16,17,18].

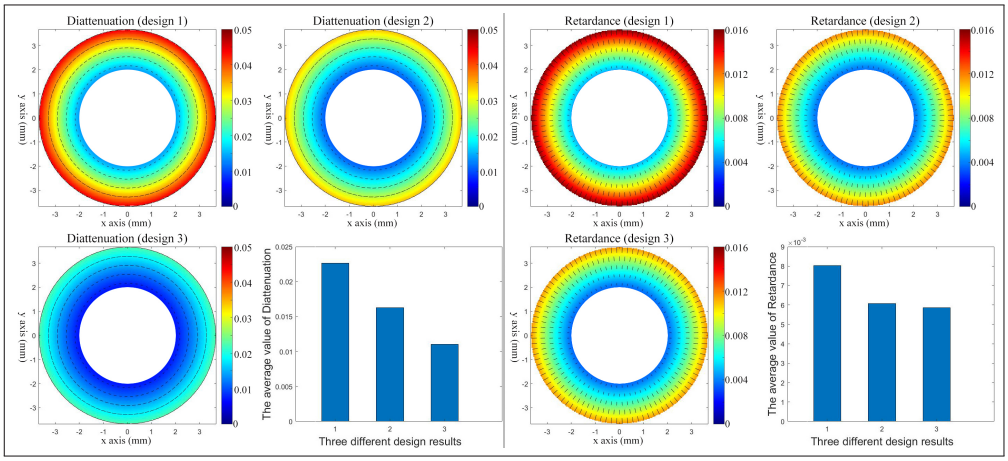

Fig. 6. Diattenuation and retardance pupil distribution of the central field of view of the three design

3.3. *Jones pupil*

Each ray through the optical system has a associated Jones matrix, which describes the polarization change. The polarization aberration function is the set of Jones matrices expressed as a function of pupil coordinates and object coordinates. The set of Jones matrices for a specified object point is called the Jones pupil, which has the form of a Jones matrix map over the exit pupil. Jones pupil is represented by a set of 2×2 Jones matrices and contains complex components with amplitude and phases, which is an image description of Equation(4). The Jones pupil of the three Cassegrain telescope systems are shown in Fig. 7.

On the whole, a small deviation of the Jones pupil from the identity matrix is due to polarization aberrations. The values of diagonal elements A_{xx} and A_{yy} are smaller than 1 because of reflection and refraction losses. The amplitudes of off-diagonal elements A_{xy} and A_{yx} are evidently smaller than those of the diagonal elements, but it causes the appearance of polarization cross-coupled

Optics EXPRESS

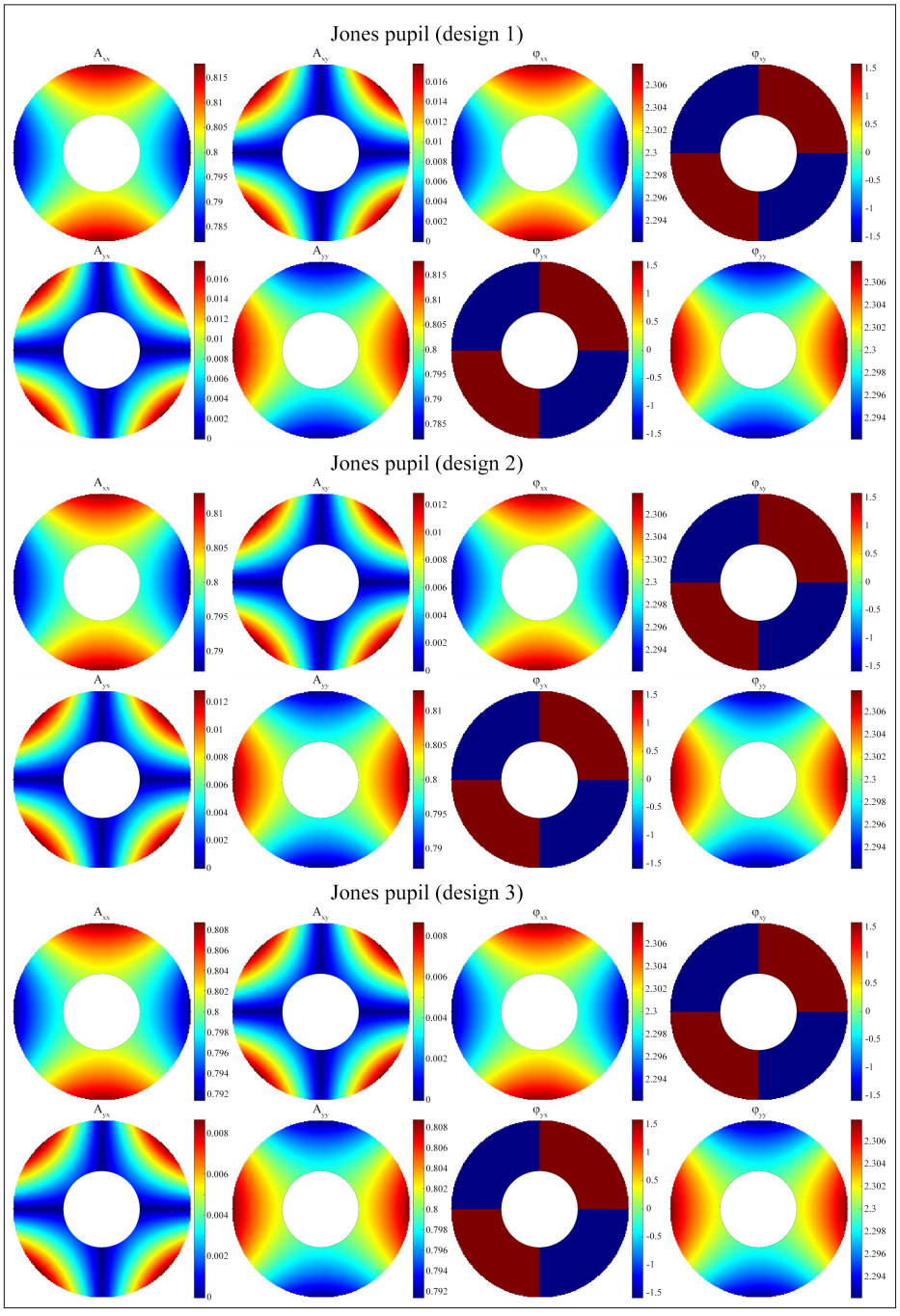

Fig. 7. Jones pupil distribution of the central field of view of the three design

Optics EXPRESS

energy. The phase of the diagonal elements ϕ_{xx} and ϕ_{yy} are continuously changing. In contrast, the off-diagonal elements ϕ_{xy} and ϕ_{yx} change discontinuously because the phase of a complex number changes by π when amplitude passes through zero due to the Fresnel's law. A_{xy} and A_{yx} are highly apodized, showing a Maltese cross pattern. At the same time, we found that after adding the lens group for optimization, the value of A_{xy} and A_{yx} are significantly reduced, which will reduce the polarization coupled-energy and reduce the influence of polarization aberration on the imaging quality.

3.4. Suppression of polarization cross-coupled energy

It is difficult to directly observe the effect of correction on the polarization cross-coupled energy with the diattenuation and retardance pupil. To calculate the total cross-coupled energy the diattenuation and retardance pupil need to be decomposed first. Johannes Ruoff and Michael Totzeck proposed an Orientation Zernike Polynomial (OZP) method as a base function representation of retardation and diattenuation, which are most relevant for vector imaging [19].

Using SVD, the Jones matrix J can be defined in terms of physical properties:

$$J = te^{i\Phi}J_{pol}(d,\theta_p)J_{ret}(\phi,\theta_r), \tag{23}$$

where J_{pol} represents the diattenuation; J_{ret} represents the retardance; t and Φ represent the mean transmission and phase, respectively; d and ϕ represent the relative amplitude difference and relative phase difference, respectively; and θ_p and θ_r represent the bright axis direction and fast axis direction [20], respectively. J_{pol} and J_{ret} can be expressed as follows:

$$J_{pol}(d,\theta_p) = \begin{bmatrix} 1+dcos(2\theta_p) & dsin(2\theta_p) \\ dsin(2\theta_p) & 1-dcos(2\theta_p) \end{bmatrix}, \tag{24}$$

$$J_{ret}(\phi,\theta_r) = \begin{bmatrix} cos\phi - isin\phi cos(2\theta_r) & -isin\phi sin(2\theta_r) \\ -isin\phi sin(2\theta_r) & cos\phi + isin\phi cos(2\theta_r) \end{bmatrix}. \tag{25}$$

We used OZP to decompose the diattenuation and retardance further:

$$J_{pol} = I + \sum_{j=1}^{\infty} C_j \cdot OZ_j, \tag{26}$$

where I is a 2×2 unit matrix, C_j is the OZP coefficient, and OZ_j is the OZP term.

We obtained the diattenuation and retardance pupil under different fields of view before and after correction, and then used OZP to decompose it; the coefficients of different OZP terms after decomposition are listed in Fig. 8.

The horizontal axis in Fig. 8 represents different OZP terms; the vertical axis represents the coefficient of the OZP term; the vertical bars of different colors in each term represent different fields of view. The first nine terms are listed in Fig. 8, the higher order terms are very close to zero, it can be seen that the diattenuation and retardance pupil is mainly decomposed into three parts:OZ_1, OZ_3 and OZ_5,

$$\begin{aligned} J_{pol} &= I + C_1OZ_1 + C_3OZ_3 + C_5OZ_5 \\ &= I + C_1\begin{bmatrix} 1 & 0 \\ 0 & -1 \end{bmatrix} + C_3\begin{bmatrix} \rho sin\theta & -\rho cos\theta \\ -\rho cos\theta & -\rho sin\theta \end{bmatrix} + C_5\begin{bmatrix} \rho^2 cos2\theta & \rho^2 sin2\theta \\ \rho^2 sin2\theta & -\rho^2 cos2\theta \end{bmatrix}. \end{aligned} \tag{27}$$

Optics EXPRESS

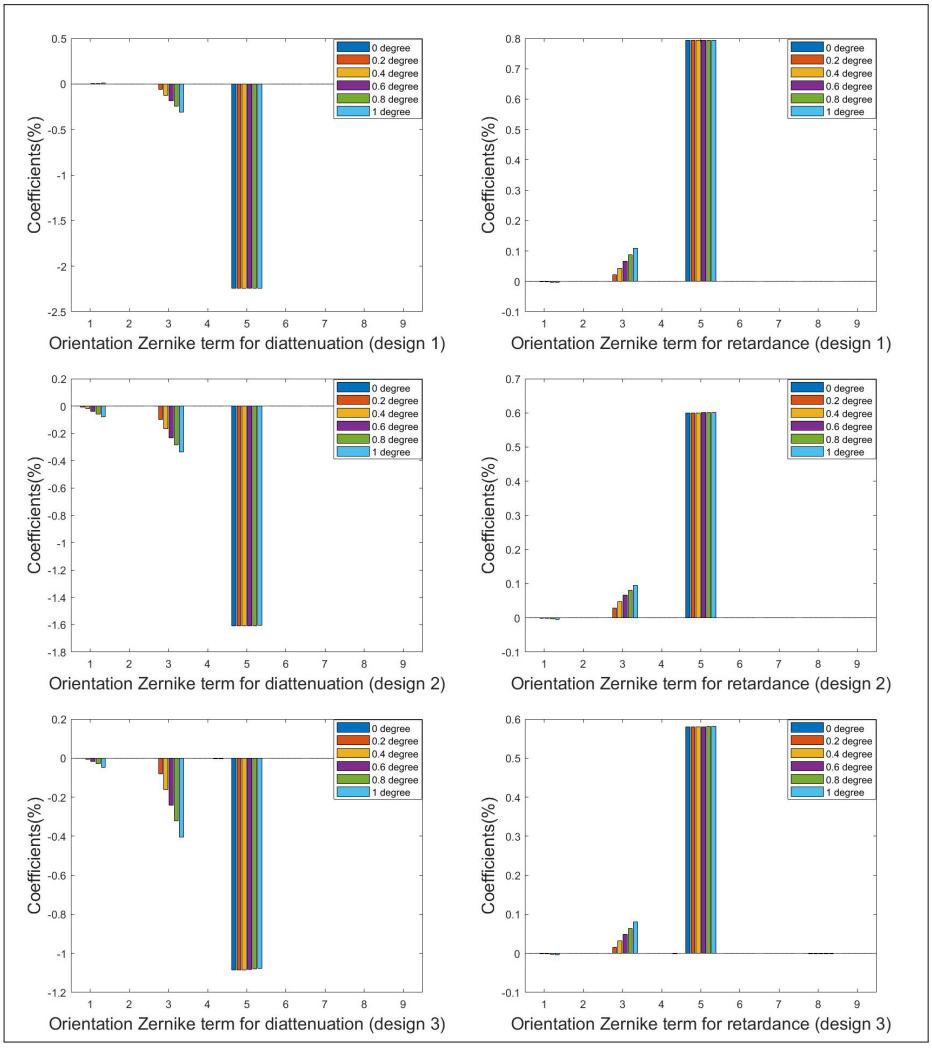

Fig. 8. OZP coefficients before and after suppression

It has been proposed to use Pauli spin matrices σ_i as a more intuitive basis for calculating the coupled energy [21]. Defining

$$\sigma_0 = \begin{bmatrix} 1 & 0 \\ 0 & 1 \end{bmatrix}, \sigma_1 = \begin{bmatrix} 1 & 0 \\ 0 & -1 \end{bmatrix}, \sigma_2 = \begin{bmatrix} 0 & 1 \\ 1 & 0 \end{bmatrix}, \sigma_3 = \begin{bmatrix} 0 & -i \\ i & 0 \end{bmatrix}, \tag{28}$$

any Jones matrix can be written as:

$$J = \sum_{i=0}^{3} a_i \sigma_i, \tag{29}$$

with complex coefficients, a_i. Examining the eigenvalues and eigenvectors of the Pauli matrices shown that σ_1 possesses linearly x/y-polarized eigenvectors, σ_2 possesses linearly 45 deg/135 deg polarized eigenvectors, whereas σ_3 corresponds to right/left circularly polarized states. The identity matrix σ_0 approximately represents the nonpolarizing part of the Jones matrix. The

Optics EXPRESS

three terms of the diattenuation pupil decomposed by OZP theory can be expressed by the Pauli matrix as

$$\begin{aligned} OZ_1 &= \sigma_1, \\ OZ_3 &= \rho sin\theta\sigma_1 - \rho cos\theta\sigma_2, \\ OZ_5 &= \rho^2 cos(2\theta)\sigma_1 + \rho^2 sin(2\theta)\sigma_2, \end{aligned} \tag{30}$$

OZ_1 is the diattenuation piston, OZ_3 the diattenuation tilt, and OZ_5 the diattenuation defocus. Figure 8 shows that the coefficients of these terms are related to the field of view. The coefficients of OZ_1 and OZ_3 are proportional to the square of the field of view, the field of view, respectively, while the coefficients of OZ_5 is almost independent of the field of view. These observations are consistent with the theory proposed by Chipman in 1987 [13]. The diattenuation and retardance pupil can be decomposed using the Pauli matrix into

$$\begin{cases} J_{dia} = \sigma_0 + (d_1 + d_3\rho\sin\theta + d_5\rho^2\cos(2\theta))\sigma_1 + (d_5\rho^2\sin(2\theta) - d_3\rho\cos\theta)\sigma_2 \\ J_{ret} = \sigma_0 - i((\Delta_1 + \Delta_3\rho\sin\theta + \Delta_5\rho^2\cos(2\theta))\sigma_1 + (\Delta_5\rho^2\sin(2\theta) - \Delta_3\rho\cos\theta)\sigma_2) \end{cases}, \tag{31}$$

d represents the coefficient of OZP decomposition for diattenuation, and Δ represents the coefficient of retardance for OZP decomposition. The fraction of incident X or Y polarization coupled into the orthogonal polarization state is determined by integrating the off-diagonal elements (the σ_2 term) magnitude squared $|J_{YX}|^2$ or $|J_{XY}|^2$ over the pupil, and normalized by π, the area of the pupil,

$$F_{XY} = \frac{\int_0^{2\pi}\int_0^1 |J_{XY}|^2\,\rho\,d\rho\,d\theta}{\int_0^{2\pi}\int_0^1 \rho\,d\rho\,d\theta} = \frac{d_3^2 + \Delta_3^2}{4} + \frac{d_5^2 + \Delta_5^2}{6}, \tag{32}$$

F_{XY} is the fraction of incident Y-polarized flux contained in the I_{XY} image integrated over the image. F_{XY} is quadratic in the tilt and defocus terms; therefore, an order of magnitude reduction in these polarization aberrations reduces the ghost brightness by two orders of magnitude. As shown in Fig. 8, the coefficient of diattenuation defocus in different fields of view after suppression has decreased overall, while the coefficient of diattenuation tilt increases, and we calculate the F_{XY} results under different fields of view, as shown in Fig. 9.

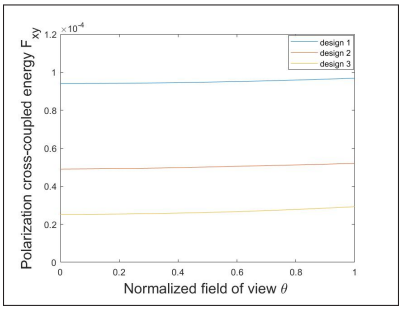

Fig. 9. Polarization cross-coupled energy before and after correction in different fields of view

It can be seen that the polarization cross-coupled energy of the system is reduced to varying degrees under the full field of view. The polarization cross-coupled energy of the center field of view is reduced by 73.18% and the polarization cross-coupled energy of the edge field of view is reduced by 69.80%.

Optics EXPRESS

3.5. Effect on modulation transfer function

The modulation transfer function (MTF) of the optical system should include the effect of polarization aberration. The distribution of flux and polarization in the image of an incoherent point source, can be described with a 4×4 Muller matrix Point Spread Matrix (PSM), this PSM is calculated by the transformation of the ARM's Jones matrices into Mueller matrix functions [22]. We calculated the PSM of the optical system using the Design 1 and Design 3 results as an example, as shown in Fig. 10.

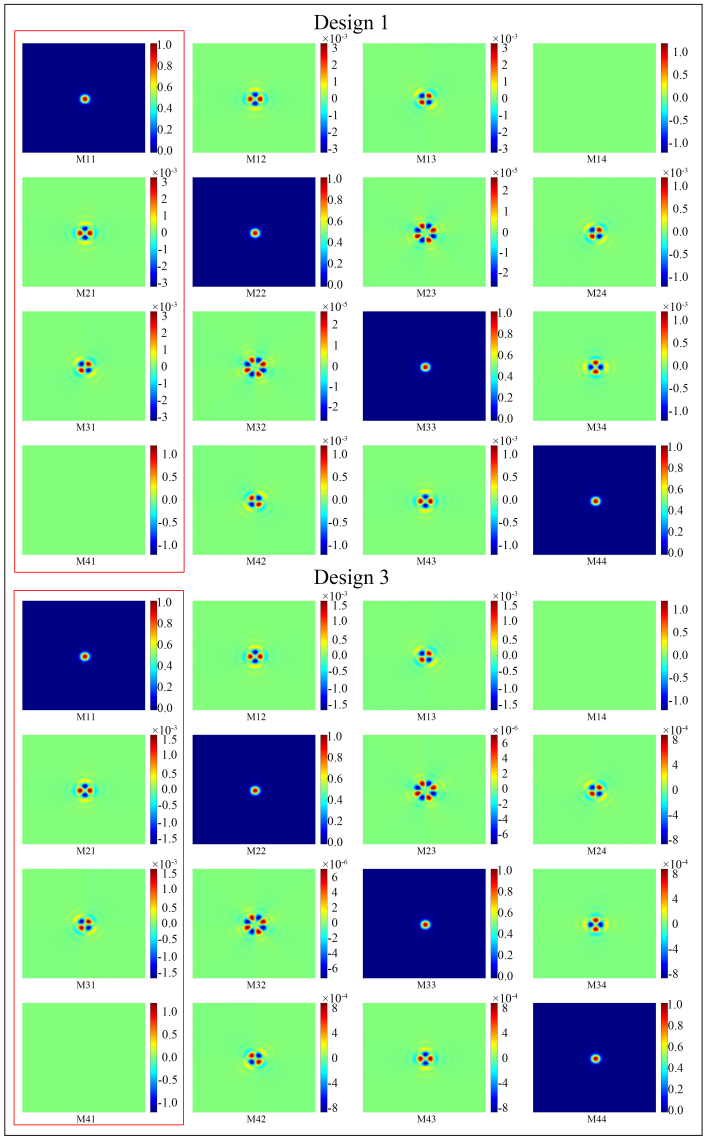

Fig. 10. The 4×4 point spread matrix for the Cassegrain telescope's on-axis image

The red box on the left (M11, M21, M31, M41) is the resultant Stokes parameter image for a collimated beam of unpolarized incident light, such as an unpolarized star. M11 is the total energy of the unpolarized light enter the optical system, for incident light with different

Optics EXPRESS

polarization states, multiply it with PSM to get the outgoing Stokes vector. By comparing the PSM of Design 1 and Design 3, we found that except for the diagonal term, the energy of other terms has been significantly reduced, which means that adding a lens group can reduce the influence of polarization aberration.

The design optimization of an optical system is a process of seeking the optimal solution under multiple constraints, and it is possible that in order to suppress polarization aberration, conventional aberration correction becomes bad. We obtained different design results by changing the weight of polarization aberration correction in the optical design software and analyzed the modulation transfer function(MTF) of the optical system. The results are shown in Fig. 11.

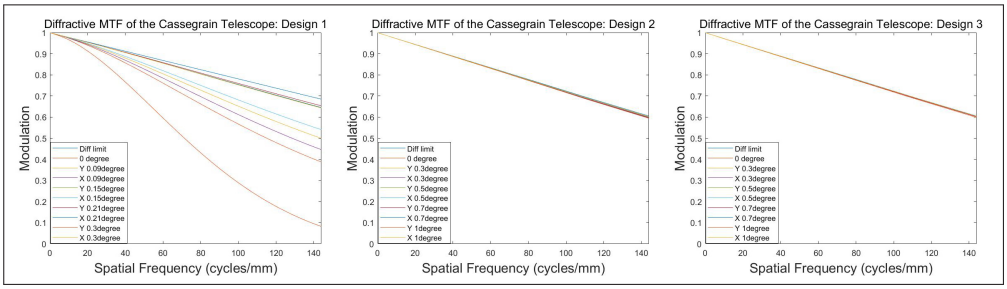

Fig. 11. The MTF of the Cassegrain telescope system of three designs

The MTF shown in Fig. 11 includes the effects of polarization aberrations when unpolarized light is incident. The energy distribution of the point spread function contains the polarization cross-coupled energy, and the calculated MTF is the absolute value of the Fourier transform of the PSF. In Design 1, the system consists of only two mirrors, and its field of view is limited to 0.3°; if the field of view is increased to 1°, its image quality will be very poor. At the same time, we can see from Fig. 11 that even if we reduce the field of view in Design 1, its MTF is still not as good as the result after adding the lens group, this is due to the lens group provide more variables for the system's aberration correction. In Designs 2 and 3, we gradually increased the weight of suppressing polarization aberration and found that under the two designs, the MTF curve has a slight fluctuation, and the overall image quality is similar, and was close to the diffraction limit. This means that we can suppress both polarization aberration and conventional aberration. The design results require the designer to achieve a balance between the polarization aberrations and other constraints.

4. Conclusions

In addition to wavefront aberrations, polarization aberrations are inevitable in any optical system. It has become an important project through reasonable design to reduce the effect of polarization aberration. The basic idea is to find materials with opposite characteristics to compensate for each other, and this study found that the diattenuation characteristic of the metal reflective coating and the glass material show the opposite characteristic. Combining the reflection and refraction optical group to design can effectively reduce the polarization aberration.

This study derived the principle of diattenuation suppression and analyzed the polarization aberration of the system before and after the addition of the refraction optical group. The simulation results show that after adding the refraction optical group, the average value of the diattenuation of the system reduces by 51.1%, and the average value of retardance is reduced by 26.3%. Diattenuation and retardance result in polarization cross-coupled energy, which was calculated before and after correction for the full field of view. The results show that the polarization cross-coupled energy reduces by 73.18% in the central field of view and 69.80%

Optics EXPRESS

in the edge of the field of view. Adding a lens group also reduces the traditional aberration, which enables expansion of the field of view of the system. The simulation results show that the combination of reflection and refraction optical groups can reduce diattenuation, thereby reducing the polarization cross-coupled energy and improving the MTF curve.

Funding. Chinese Academy of Sciences (CXJJ-20S04, YJKYYQ20190083); National Natural Science Foundation of China (61905242).

Disclosures. The authors declare that they have no conflicts of interest.

Data availability. Data underlying the results presented in this paper are available in Code 1 Ref. [15].

References

1. J. B. Breckinridge, W. S. T. Lam, and R. A. Chipman, "Polarization aberrations in astronomical telescopes: the point spread function," Publ. Astron. Soc. Pac. **127**(951), 445–468 (2015).
2. J. Breckinridge and R. Chipman, "Telescope polarization and image quality: Lyot coronagraph performance," in *Space Telescopes and Instrumentation 2016: Optical, Infrared, and Millimeter Wave*, vol. 9904 (SPIE, 2016), pp. 474–489.
3. J. Luo, X. He, K. Fan, and X. Zhang, "Effects of polarization aberrations in an unobscured off-axis space telescope on its psf ellipticity," Opt. Express **28**(25), 37958–37970 (2020).
4. J. Breckinridge, M. Kupinski, J. Davis, B. Daugherty, and R. Chipman, "Terrestrial exoplanet coronagraph image quality: study of polarization aberrations in habex and luvoir update," in *Space Telescopes and Instrumentation 2018: Optical, Infrared, and Millimeter Wave*, vol. 10698 (SPIE, 2018), pp. 429–445.
5. M. Totzeck, P. Graupner, T. Heil, A. Gohnermeier, O. Dittmann, D. Krahmer, V. Kamenov, J. Ruoff, and D. Flagello, "How to describe polarization influence on imaging," in *Optical Microlithography XVIII*, vol. 5754 (SPIE, 2005), pp. 23–37.
6. B. Geh, J. Ruoff, J. Zimmermann, P. Gräupner, M. Totzeck, M. Mengel, U. Hempelmann, and E. Schmitt-Weaver, "The impact of projection lens polarization properties on lithographic process at hyper-na," in *Optical Microlithography XX*, vol. 6520 (SPIE, 2007), pp. 186–203.
7. G. R. McIntyre, J.-W. Kye, H. J. Levinson, and A. R. Neureuther, "Polarization aberrations in hyper-numerical-aperture projection printing: a comparison of various representations," J. Micro/Nanolithogr., MEMS, MOEMS **5**(3), 033001 (2006).
8. M. Shribak, S. Inoue, and R. Oldenbourg, "Polarization aberrations caused by differential transmission and phase shift in high-numerical-aperture lenses: theory, measurement, and rectification," in *Collected Works Of Shinya InouÉ: Microscopes, Living Cells, and Dynamic Molecules (With DVD-ROM)*, (World Scientific, 2008), pp. 857–868.
9. S. Banerjee, R. Chipman, and Y. Otani, "Simultaneous balancing of geometric transformation and linear polarizations using six-fold-mirror geometry over the visible region," Opt. Lett. **45**(9), 2510–2513 (2020).
10. W. S. T. Lam and R. Chipman, "Balancing polarization aberrations in crossed fold mirrors," Appl. Opt. **54**(11), 3236–3245 (2015).
11. W. Jia, W. He, Q. Wang, R. Wang, Z. Xiong, and L. Zhang, "Polarization aberrations corrections and polarization-dependent imaging quality analysis in polarization lidars," Opt. Commun. **495**, 127106 (2021).
12. M. Born and E. Wolf, *Principles of optics: electromagnetic theory of propagation, interference and diffraction of light* (Elsevier, 2013).
13. R. A. Chipman, "Polarization aberrations," Ph. D. Thesis (1987).
14. J. P. McGuire and R. A. Chipman, "Diffraction image formation in optical systems with polarization aberrations. i: Formulation and example," J. Opt. Soc. Am. A **7**(9), 1614–1626 (1990).
15. C. Jiang, "Codev file contain design results 2 and 3," figshare, (2022), https://doi.org/10.6084/m9.figshare.21213071.
16. J. Kye, G. McIntyre, Y. Norihiro, and H. J. Levinson, "Polarization aberration analysis in optical lithography systems," in *Optical Microlithography XIX*, vol. 6154 (SPIE, 2006), pp. 144–154.
17. J. Ruoff and M. Totzeck, "Orientation zernike polynomials: a useful way to describe the polarization effects of optical imaging systems," J. Micro/Nanolithogr., MEMS, MOEMS **8**(3), 031404 (2009).
18. J. Ruoff and M. Totzeck, "Using orientation zernike polynomials to predict the imaging performance of optical systems with birefringent and partly polarizing components," in *International Optical Design Conference 2010*, vol. 7652 (SPIE, 2010), pp. 597–610.
19. T. Heil, J. Ruoff, J. T. Neumann, M. Totzeck, D. Krähmer, B. Geh, and P. Gräupner, "Orientation zernike polynomials: a systematic description of polarized imaging using high na lithography lenses," in *Lithography Asia 2008*, vol. 7140 (SPIE, 2008), pp. 287–298.
20. X. Xu, W. Huang, and M. Xu, "Orthogonal polynomials describing polarization aberration for rotationally symmetric optical systems," Opt. Express **23**(21), 27911–27919 (2015).
21. C. Whitney, "Pauli-algebraic operators in polarization optics," J. Opt. Soc. Am. **61**(9), 1207–1213 (1971).
22. J. W. Hovenier, C. V. Van der Mee, and H. Domke, *Transfer of polarized light in planetary atmospheres: basic concepts and practical methods*, vol. 318 (Springer Science & Business Media, 2004).